

Impact of warmer climate on Lake Geneva water-temperature profiles

Marjorie Perroud and Stéphane Goyette

Climatic Change and Climate Impacts (C³I), University of Geneva, Site de Battelle/D, Chemin de Drize 7, 1227 Carouge/GE, Switzerland.

Received 2 Feb. 2009, accepted 17 Sep. 2009 (Editor in charge of this article: Kai Myrberg)

Perroud, M. & Goyette, S. 2010: Impact of warmer climate on Lake Geneva water-temperature profiles. *Boreal Env. Res.* 15: 255–278.

The impact of climate warming caused by the increase of greenhouse gases in the atmosphere on the thermal profiles of Lake Geneva, Switzerland, is investigated using a k - ϵ turbulence lake model. To assess the thermal response of this lake, two sets of 130-year time series of hourly meteorological variables are used to drive the lake model. In the control simulation, the lake model is driven by a series representative of the period 1981–1990, and in the perturbed experiment, deltas derived from outputs of the HIRHAM Regional Climate Model run under the IPCC A2 scenario in the framework of the 5th EU programme PRUDENCE, have been used. Changes in the lake water temperature profiles indicate an increase in monthly epilimnic and hypolimnic temperatures of 2.32–3.8 °C and 2.2–2.33 °C, respectively. The rising of epilimnic temperatures corresponds to 55%–98% of the monthly increase in air temperature. The stratification period lasts longer and the lake stability increases. Thus the lake is likely to retain its mixing regime, but this will be of shorter duration.

Introduction

The mean global surface warming of the earth caused by the increase of greenhouse gas (GHG) concentrations over the 20th century (0.74 °C from 1906 to 2005, IPCC 2007) has induced a wide-range of impacts in many parts of the world (Alcamo *et al.* 2007). In lakes, thermal response to recent atmospheric warming reveals that the first signs of change are already observed in many regions. Most studies agree on an increase in the temperature of surface waters, and sometimes also at the bottom of lakes. In all cases, the temperature increase is observed to be higher in the epilimnion than in the hypolimnion; there is currently an earlier onset and strengthening of

the summer stratification, and a shorter duration of ice cover during the freezing season (Robertson and Ragotzkie 1990, Schindler *et al.* 1996, King *et al.* 1997, McCormick and Fahnenstiel 1999, Peeters *et al.* 2002, Livingstone 2003).

GHG emissions are likely to increase at an accelerating rate during coming decades with stronger impacts than those until now (IPCC 2007). Estimates of warming vary largely due to the GHG emissions scenario (cf. SRES — the Special Report on Emission Scenarios; Nakicenovic *et al.* 2000) as well as to the climate model used. In Europe for instance, models project an increase of 1–4 °C for the SRES B2 scenario and 2.5–5.5 °C for the A2 scenario in the 2070–2099 timeframe as compared with the baseline, or

“current” (1961–1990) climate (Alcamo *et al.* 2007). An increase in mean global temperature of 1.5–2.5 °C may also induce changes in ecosystem structure and function, ecological interactions between species and their geographical ranges, often with negative consequence for biodiversity and ecosystems (Fischlin *et al.* 2007). Impacts of a warmer climate on the thermal evolution of lakes and therefore on organisms dependent on water temperature thus need to be investigated.

In this study, particular attention has been devoted to Lake Geneva, a warm and deep monomictic lake in which effects of warmer meteorological conditions have recently been observed (Lazzarotto *et al.* 2004, Dokulil *et al.* 2006). Since the early 1970s, an increase of more than 1 °C in the annual mean surface temperature has been recorded, as shown at a depth of 5 m (Lazzarotto *et al.* 2004). In addition, bottom temperatures increased progressively from 4.5 °C measured in the 1960s to the maximum of 5.98 °C measured in 2002. The occurrence of occasional cold winters cooled water layers near the bottom, but their temperature have never reverted to the values observed in the 1960s. Other studies also highlight indirect effects of changes due to warming on phytoplanktonic community composition (Anneville *et al.* 2005) and on fish communities (Gerdeaux 2004, Gillet and Quetin 2006).

With the purpose of examining the thermal evolution of Lake Geneva in the long term, a k - ϵ one-dimensional numerical lake model, called SIMSTRAT (Goudsmit *et al.* 2002), has been chosen to simulate water temperature profiles of this large lake. To explore how Lake Geneva might be affected by changes in current and future climate conditions, meteorological data used to drive the model have been perturbed using the outputs of the HIRHAM regional climate model (RCM), described by Christensen *et al.* (1998). A method, referred to as the decile method, based on the difference in the distribution of meteorological variables between current and future periods will be presented. This latter is broadly similar to previous methods in that meteorological data are modified according to differences between future and current climates simulated by global circulation models (GCM)

or by RCMs. However, the method differs in the manner how perturbations are segmented (according to the deciles from a distribution, i.e. at each 10% increment of the probability distribution function rather than using just the average temperature difference).

The response of a deep warm monomictic lake to expected changes in weather conditions needs to be analysed in the long term, especially when deep mixing does not cool deeper layers at regular time intervals. Indeed, the heat transported downward and stored over several years is a determinant for bottom temperatures (Coats *et al.* 2006). For such water bodies, a long historical meteorological dataset is useful to study the trend in deep waters when daily variability is taken into account (Peeters *et al.* 2002). Unfortunately, long time series tend to be rare and thus strategies for running long-term simulations need to be developed. For Lake Geneva, hourly meteorological data required to run the lake model have been collected for the past 30 years, but only 10 years (1981–1990) cover the period prior to the intense warming trend of the past 20 years. A meteorological data generator in which variable distributions match the observations has thus been developed that allows running numerical simulations over several decades. This generator is designed to reproduce the mean and variability of the current meteorological conditions. The simulated water temperature profiles, when the SIMSTRAT lake model is driven by meteorological observations, are validated against observed profiles. Next, the weather generator is used to produce a series of pseudo-random data that will serve to drive a long simulation representing the current climate conditions. In addition, this long series of pseudo-random data representative of the current conditions will be perturbed using the decile method and then be used to drive simulations, as a proxy for future climate conditions. Thermal properties of Lake Geneva as simulated for the last decade of the 21st century is assessed by analysing monthly changes in epilimnic and hypolimnic water temperatures. Variations in the onset of the stratification, depth of the thermocline and strength of the stratification will serve to explain differences in the warming of surface and bottom layers. Particular attention will also be paid to the way radiative, sensible and latent

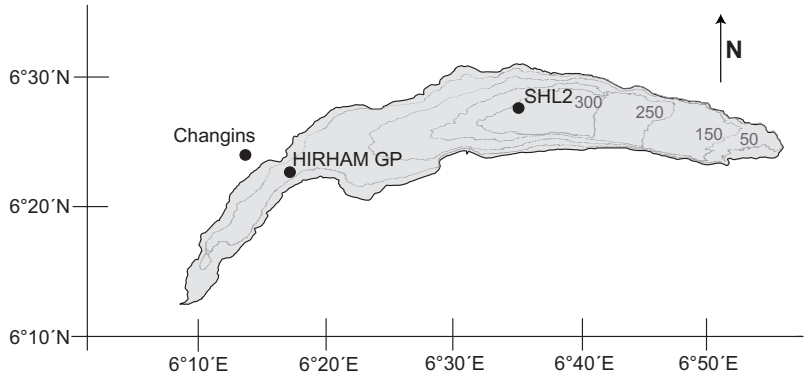


Fig. 1. Map of Lake Geneva with locations of the meteorological station Changins, the HIRHAM RCM grid point over Lake Geneva, and the lake sounding station SHL2.

heat fluxes evolve with respect to changes in air temperature and surface water temperature. A final discussion will then relate the evolution of thermal properties and stratification in Lake Geneva to results from other studies concerned with global warming in other lakes.

Material and methods

Study site and lake data

Lake Geneva, the deepest in western Europe (309 m), is a large water body located in the western perialpine area of Switzerland, bordered by France on the southern shore. It is composed of two basins, a main basin, referred to as the “Grand Lac”, that represents more than 96% of the total water volume and an adjacent shallower and narrow downstream basin that forms the “Petit Lac” (Fig. 1). It is considered a warm monomictic lake even though overturns rarely reach the bottom of the “Grand Lac” (Lazzarotto *et al.* 2006, Lazzarotto and Rapin 2007).

Within the framework of a monitoring program coordinated by the International Commission for the Protection of Lake Geneva (CIPEL), discrete measurements of water temperature profiles and bio-chemical properties are collected twice a month at station SHL2, located at its deepest point by the French National Institute for Agricultural Research (INRA). As sampling depths vary slightly with time, only depths of 0, 2.5, 5, 7.5, 10, 15, 20, 30, 35, 50, 100, 150, 200, 250, 300 meters (Database INRA of Thonon-Les-Bains, Data CIPEL) are employed in the following analysis.

Lake model

For climatological applications, one-dimensional (1D) lake models are usually used because of their computational efficiency and the realistic temperature profiles that they produce. A wide range of 1D lake models have proven efficient in reproducing multiple aspects of thermal profiles in large lakes in a stand-alone mode (Hostetler and Bartlein 1990, Boyce *et al.* 1993, Peeters *et al.* 2002, Perroud *et al.* 2009). Depending on the numerical schemes used, we may find eddy-diffusion models (Orlob and Selna 1970, Henderson-Sellers *et al.* 1983), turbulence-based models (Kraus and Turner 1967, Imberger *et al.* 1978), in particular $k-\epsilon$ models (Burchard and Baumert 1995, Goudsmit *et al.* 2002, Stepanenko and Lykosov 2005), mixed-layer models (Stefan and Fang 1994, Goyette *et al.* 2000), or models based on similarity theory (Mironov 2008, Mironov *et al.* 2010). If turbulent processes such as those generated by shear stress or density instabilities are generally numerically resolved in 1D models, it is true that many processes explicitly implemented in 3D lake models are missing (Bennett 1978, Kelley *et al.* 1998, Hodges *et al.* 2000). 1D lake models may miss for instance horizontal advection or mixing induced by progressive or long standing waves, and particularly on large lakes when the effects of earth rotation are neglected (e.g. Kelvin seiches). However, 3D lake models present two main disadvantages; first they are too time-consuming for century-scale applications and secondly the small number of meteorological stations recording data around the lake cannot provide the adequate boundary conditions required for simulations

with 3D models. Despite the obvious limitations associated with the use of 1D lake models, the simulation of thermal profiles in Lake Geneva at SHL2 was previously assessed using four different 1D lake models (Perroud *et al.* 2009). Two of them were clearly capable of simulating water temperature profiles over 10 independent annual cycles. Indeed, these latter had the advantage of parameterizing 3D processes, i.e., the vertical mixing due to the effects of seiche on the metahypolimnion.

SIMSTRAT (Goudsmit *et al.* 2002, Peeters *et al.* 2002), has been used in this study to examine the evolution of temperature profiles in a changing climate. In this model, turbulent diffusivity is estimated from the production k and dissipation ε of turbulent kinetic energy, TKE. Apart from buoyancy and shear, SIMSTRAT extends the production of TKE to mixing processes from seiche motion, i.e., from the release of TKE by friction on the bottom boundary. The version employed in this study has different boundary conditions from those of Goudsmit (2002). First, a new formulation for albedo has been intro-

duced to account for the time-dependent solar zenith angle. Secondly, the varying wave height has been parameterized by using two empirical equations for the drag coefficient c_D , one to relate increasing wind speed to higher c_D and the other for variation of c_D with wind speed below 3 m s^{-1} . Details on these modifications are given in Perroud *et al.* (2009). In order to calculate the evolution of water temperature profiles, the energy budget and wind stress forcing need to be estimated at each time step. The energy components are thus either given as input to the model if they are measured to the meteorological station close to the lake, or deduced from a given parameterization (Table 1). The model time step is set at 10 minutes for a vertical grid spacing of 0.75 m.

Meteorological data collected from 1980 to 2006 at the land station Changins (Fig. 1) are supplied by the Automatic Network (ANETZ) of the Federal Office of Meteorology and Climatology, Meteoswiss (Bantle 1989). The following are used as inputs to the model: hourly values of air temperature, T , horizontal wind magnitude, v , wind direction, dir , relative humidity, RH ,

Table 1. Energy fluxes at the water–atmosphere interface and calibration parameters.

Model parameter	Value	Unit	Remarks
$L\downarrow$	$(1 - r_a)\varepsilon_a\sigma T_a^4$	W m^{-2}	downward atmospheric longwave
r_a	0.03	–	reflection of infrared radiation from water
ε_a	$1.24(1 + 0.17C^2)\left(\frac{e_a}{T_a}\right)^{\frac{1}{7}}$	–	atmospheric emissivity
C	–	–	cloud coverage
σ	5.67×10^{-8}	$\text{W m}^{-2} \text{K}^{-4}$	Stefan-Boltzmann constant
T_a	–	K	absolute atmospheric temperature
e_a	–	hPa	atmospheric water-vapour pressure
$L\uparrow$	$-\varepsilon_w\sigma T_w^4$	W m^{-2}	emitted longwave
ε_w	0.97	–	longwave emissivity of water
T_w	–	K	absolute temperature of water
Q_h	$Bf_u(T_w - T_a)$	W m^{-2}	sensible heat flux
f_u	$4.4 + 1.82\sqrt{U_{10}^2 + V_{10}^2} + 0.26(T_w - T_a)$	$\text{W m}^{-2} \text{K}^{-1}$	transfer function
B	0.61	–	Bowen ration
Q_e	$f_l(e_w - e_a)$	W m^{-2}	latent heat flux
e_w	$f_w \times 10 \frac{0.7859 + 0.03477T_w}{1 + 0.00412T_w}$	hPa	water vapour saturation at T_w
f_w	$0.61[1 + 10^{-6}P(4.5 + 6 \times 10^{-5}T_w^2)]$	$\text{W m}^{-2} \text{hPa}^{-1}$	transfer function
P	–	hPa	air pressure

* T_a has been adjusted in this study with respect to conditions at the lake surface, $T_a = T_L$.

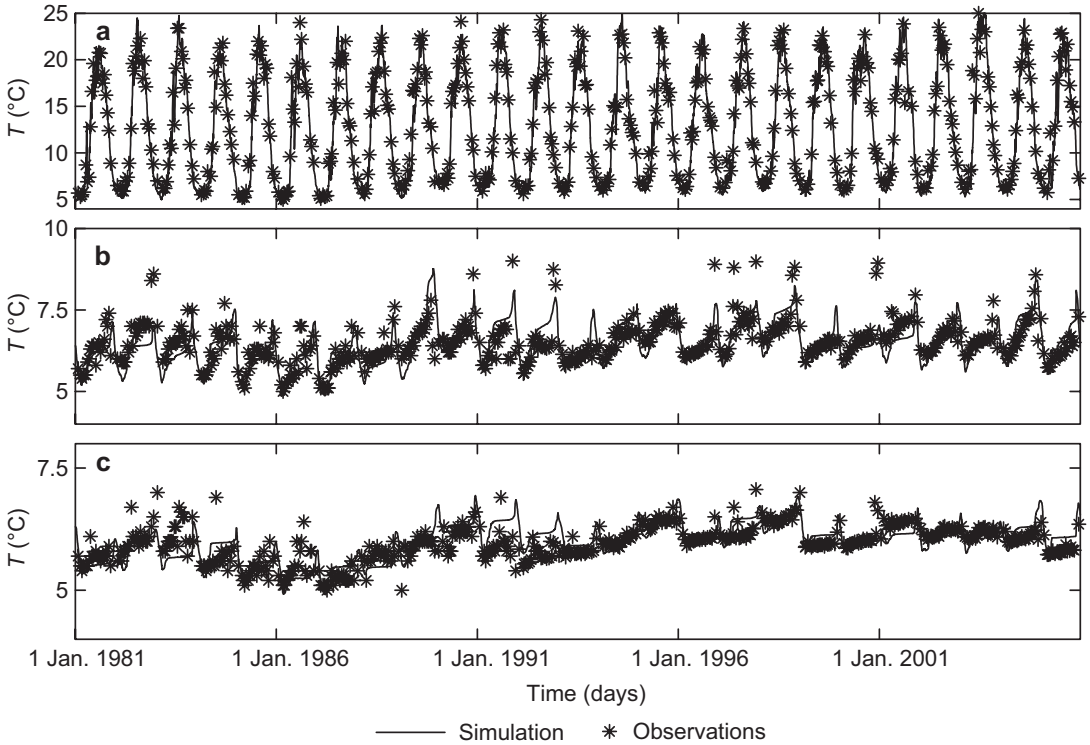


Fig. 2. SIMSTRAT simulated water temperatures and observed temperatures at (a) the surface, (b) 10-m depth and (c) 100-m depth from 1 January 1981 to 31 December 2005.

surface pressure, P , downward solar radiation, S_{\downarrow} , and cloud cover, C . T is adjusted to account for the difference of elevation $\Delta z = z_{\text{station}} - z_L$ between the land station, z_{station} , and the lake reference, z_L , as follows:

$$T_L = T_{\text{station}} + \Delta z \gamma \quad (1)$$

where T_L is the temperature over the lake, T_{station} is the temperature at Changins, and γ is the vertical lapse rate fixed at 6.5 K km^{-1} . A scaling factor is also applied to v in order to be more representative of the conditions over the lake open water (Perroud *et al.* 2009).

The penetration of S_{\downarrow} through the water column is modulated by the light extinction coefficient, K_e , from the Beer-Lambert law. The euphotic depth (1% of surface light intensity) is calculated from bi-monthly measurements of the secchi disk depth. Values are then linearly interpolated to cover the missing daily data.

To ensure that the model does not drift when run over a long period, a simulation with a

26-year meteorological record is first carried out. The simulation is initialized with the last temperature profiles taken at SHL2 in December 1980 and is then run through to 31 December 2005. Since the model has been calibrated for Lake Geneva for individual years (Perroud *et al.* 2009), a new calibration procedure covering continuous years is completed by adjusting the two empirical parameters, α and q , both used in the algorithm of boundary mixing and related to the seiche activity. Calibration is undertaken for two 5-year periods (1981–1986 and 2000–2005) by minimizing the root mean square error (RMSE) between observed and simulated water temperatures. The values are first adjusted to fit the first period before being tested against the second dataset for validation. The temperature profiles simulated over 26 years show that the model remains remarkably stable and reproduces fairly accurately the temperature variations at all depths (Fig. 2). A statistical analysis applied on more than 500 soundings collected at SHL2 indicates that the RMSEs are below $1.5 \text{ }^{\circ}\text{C}$, except

between 10 m and 15 m where errors are likely due to difficulties to locate the exact depth of the thermocline. The mean error ME and the standard deviation σ are: -0.91 °C and 1.16 °C at the surface, -0.05 °C and 1.63 °C at 10 m, -0.24 °C and 0.53 °C at 50 m, and lower than -0.2 °C and 0.3 °C below, respectively (Table 2).

Model inputs for long term simulations

Current data set

In order to capture the evolution of the thermal signal in the deep hypolimnion of this monomictic lake, it is necessary to drive the model with atmospheric inputs over a longer period. The meteorological dataset that is created to run the model in the long term needs to have similar statistics to those of the reference period of 1981–1990. In addition, the long term average water temperature profiles simulated by SIMSTRAT, also need to be fairly similar to those obtained from the 10 years of observation. A novel concept thus needs to be developed to fulfil two requirements: these long series of data will (1) help identify meteorological variables whose variability is essential in reproducing water temperature profiles, and (2) generate longer series

Table 2. Mean error (°C), standard deviations (°C) of the error and root mean square error (°C) between observed and simulated water temperature (°C) profiles from December 1980 to December 2005.

Depth	Mean error	Standard deviation	Root mean square error
Surface	-0.91	1.16	1.47
2.5 m	-0.74	1.09	1.31
5 m	-0.33	1.35	1.38
7.5 m	-0.15	1.43	1.44
10 m	-0.05	1.63	1.63
15 m	-0.22	1.54	1.56
20 m	-0.26	1.22	1.25
30 m	-0.25	0.93	0.96
35 m	-0.38	0.78	0.87
50 m	-0.24	0.54	0.59
100 m	-0.20	0.29	0.35
150 m	-0.16	0.23	0.28
200 m	-0.07	0.23	0.24
250 m	-0.01	0.27	0.27
300 m	0.03	0.29	0.29

of realistic variables to drive SIMSTRAT to ensure that the model water temperatures do not drift with time.

First, a one-year sequence of the hourly mean meteorological variable \bar{x}_i ($i = [T, v, RH, dir, C, S\downarrow]$) is produced by averaging hourly data covering the 10-year period. \bar{x}_i is then concatenated 10 times to produce a series of same length as the period of observations. Then, simulated water temperature profiles driven with current observations and with hourly average observations are compared. These results show that water temperatures are generally underestimated (Fig. 3a). In fact, hourly averages tend to reduce the supply of heat penetrating into the water column.

To analyse the importance of a variable on the fluxes that generate the necessary heat transfer with depth, hourly averages are replaced in turn with the original time series. Results indicate that the variability of the winds only, the other variables keeping their hourly mean values, decreases the RMSE by 88% and the mean error is reduced at all depths of the profile (Fig. 3a). In order to generate a long sequence of winds, a weather generator is used to create a pseudo-random time series to avoid reproducing periodic events.

Second, since potential changes in T and RH will be investigated in the next section, their variability will also be reproduced with the generator.

The pseudo-random meteorological data generation consists in the creation of meteorological variables m_i ($i = [v, dir, T, RH]$) whose distribution properties are similar to those of the current observations. This means that the monthly mean distribution μ_D , the intra-day standard deviation, σ_{IAD} , and the inter-day standard deviation, σ_{IED} , of a variable must be similar to the 10-year observations. The generation of pseudo-random data (Appendix) follows basically the same procedure for v , RH and T and data finally produced by the generator fits observations in terms of μ_D , σ_{IAD} and σ_{IED} (Fig. 4).

A 100-year sequence of m_i has been created in order to validate this method for the model's ability to reproduce the water temperature profile (mean and variance), when driven by such time series. Profiles thus simulated are averaged to produce 10 decadal daily profiles. Each of

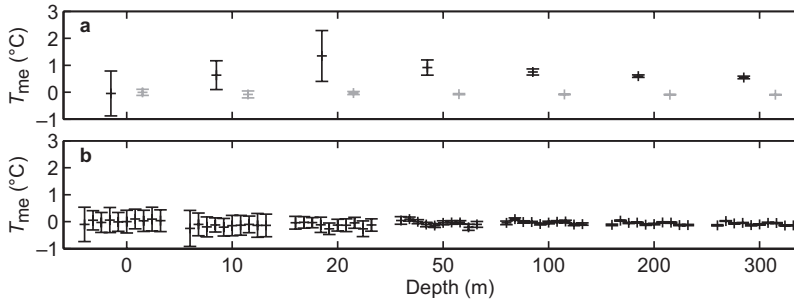


Fig. 3. (a) Mean error and standard deviation for decadal mean simulated water temperatures when driven with current observations (1981–1990) and hourly average observations (first error bar), except for wind (second error bar) at different depths. (b) Mean error and standard deviation of mean for simulated water temperatures when driven with current observations (1981–1990) and 10 individual decadal datasets of mean daily values of $S\downarrow$ and C , and pseudo-random series of v , dir , T and RH .

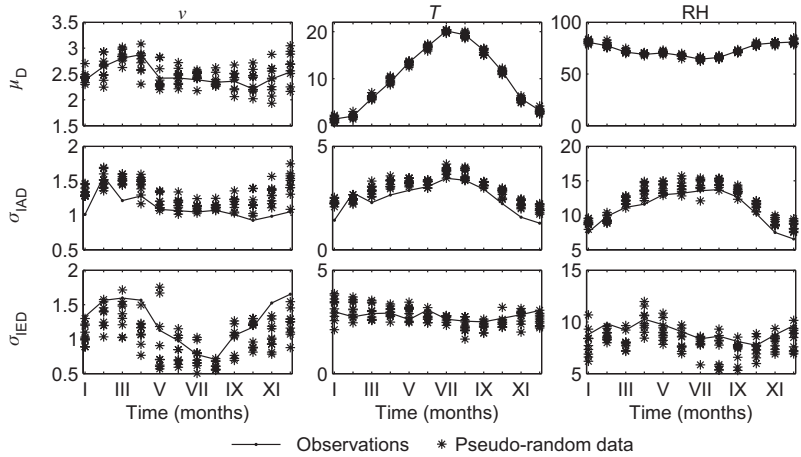


Fig. 4. Monthly means (μ_D) (upper row), monthly mean intra-day standard deviation (σ_{IAD}) (middle row), and inter-day standard deviation (σ_{IED}) (lower row) of 10 years of pseudo-random v , T and RH compared individually with the averaged monthly means recorded at Changins during 1981–1990 (upper row).

them reproduces accurately decadal mean daily profiles and lies inside their daily extrema found within the 10-year period (Fig. 5). Maximum mean errors ($< 0.25\text{ }^\circ\text{C}$) are found in the metalimnic layers, e.g. at 10 m below the surface (Fig. 3b). It is noticed that no systematic drift appears (Fig. 6). Mean daily values of $S\downarrow$ and C , combined with pseudo-random v , dir , T and RH thus forms a dataset suitable to drive SIMSTRAT in order to simulate water temperature profiles representative of the current period over long period of time.

Data set perturbed using the decile method

To assess changes in the water temperature of Lake Geneva in response to a changing climate, daily mean outputs obtained from the HIRHAM

Danish Regional Climate model used in the framework of the 5th EU programme PRUDENCE (Christensen *et al.* 1998) are taken into account. The hourly observed meteorological input variables driving the lake model are thus perturbed according to changes diagnosed with the HIRHAM outputs. This model provides two sets of daily meteorological variables, covering respectively the periods of 1961–1990 and 2071–2100, at 21 grid points over Switzerland. The atmospheric CO_2 concentrations projected in the model follow the IPCC A2 emissions scenario (IPCC 2001).

In many climate studies, physical characteristics prescribed at grid points as compared with those at the observation site (e.g., land cover) as well as low archival frequency of GCM data prevent using RCM outputs as input data to run subsequent models. Therefore, the approach

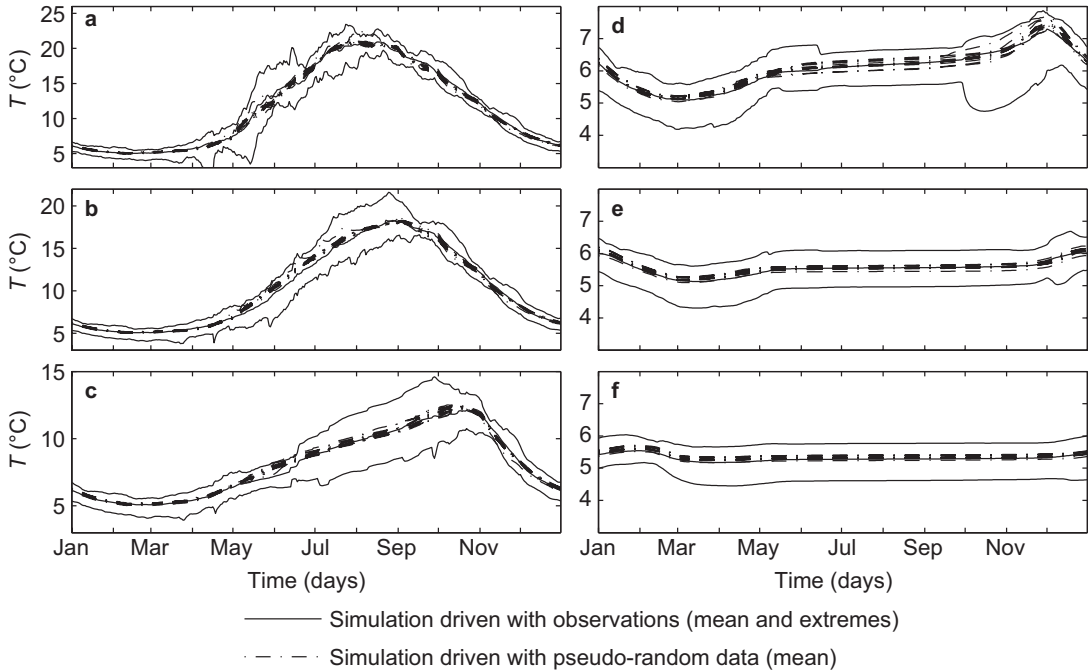


Fig. 5. Mean daily water temperature profiles per decade are obtained from a 100-year simulation driven with pseudo-random v , dir , T and RH and observation (1981–1990) at (a) the surface, (b) 10-m depth, (c) 20-m depth, (d) 50-m depth, (e) 100-m depth and (f) 200-m depth.

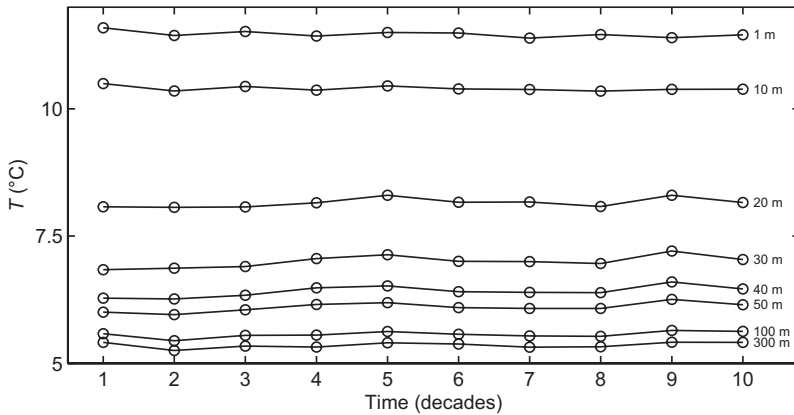


Fig. 6. Mean decadal temperature profiles obtained from a 100-year simulation driven with pseudo-random series of v , dir , T and RH .

that is usually proposed to investigated climate forcing on environmental systems consists in adding a Δ increment to observations, or a ratio r obtained by linking past and future outputs from a RCM (Boyce *et al.* 1993, Mortsch and Quinn 1996, Stefan *et al.* 1998, Fang and Stefan 1999). As shown in Fang and Stefan (1996, 1999), Δ or r are not uniform throughout the year and may vary from one month to another. To better represent the time change of the data over the year,

Δ or r should vary on a seasonal or monthly basis since trends are not the same. Based on this approach, the method for the present study can thus be described as follows:

$$\phi_i = x_i + \lambda\Delta \tag{2}$$

where ϕ_i is the hourly meteorological variables expected in the future, $\lambda = [0, \dots, 1]$ is an empirical scaling parameter and Δ is the monthly dif-

ference between HIRHAM future and current data. Jungo and Beniston (2001) showed that minima, maxima and mean temperatures will not change in the same way. A single Δ may omit the large variability of this parameter moving away from the mean. Uhlmann *et al.* (2009) proposed to calculate several forms of Δ for the same period, that is Δ 's that characterize the minimum, maximum and mean temperatures. In this study, estimates of Δ follow a more detailed approach than that of Uhlmann *et al.* (2009). Monthly data distribution of the current and future periods are divided into deciles, d_i ($i = 1, \dots, 10$); values delimited by the same two deciles are grouped to form a class and then averaged to produce one mean value per class. Ten values per month and per variable are thus obtained for the current period and an equivalent number of values for the future period. Differences between respective classes of deciles for the first and second period produce 10 different values of Δ per month. The Δ produced for the smallest values of a distribution ($< d_1$) may be rather different to the Δ produced for the highest values ($> d_9$). Observed data are scaled by the Δ corresponding to the class (defined by d_i from HIRHAM data distribution for the period 1961–1990) in which they belong.

As regards the monthly Δ determined for the five input variables (Table 3) driving the lake model, the air temperature T and dew point temperature T_d at screen level for the grid point over Lake Geneva are the most sensitive to future modifications. As RH is not provided by HIRHAM outputs, T_d is used. Perturbations to

observed hourly data will thus be applied only to T and T_d . The adjustment of variables for the difference in elevation $\Delta z = z_H - z_L$ is made as follows:

$$T_L = T_H + \Delta z \gamma \quad (3)$$

$$RH_H = f(T_H, T_{dH}) \quad (4)$$

$$T_{dH} = f(T_L, RH_H) \quad (5)$$

with the subscript H and L, for the HIRHAM and the lake variables, respectively. Monthly bias of T and T_d between the HIRHAM variables and observations, Δ_{HL} , are calculated. While monthly Δ_{HL} is low for T (± 1 °C), HIRHAM generally overestimates the moisture level of the atmosphere (Δ_{HL} for $T_d = [1.5$ °C, 4.5 °C] from January to August). Δ_{HL} is considered thereafter.

Unlike T , Δ for T_d cannot be deduced from the distribution of T_d only. The same value of T_d may indicate that the atmosphere is saturated (if T equals T_d) or unsaturated (if T is higher than T_d). The larger the difference between T and T_d is, the drier the conditions are. Thus, changes in RH are obtained by calculating monthly Δ on the basis of the distribution of $T - T_d$. Even though current data distribution is different for HIRHAM and the Changins meteorological observing site, it is hypothesised that Δ for T_d , henceforth ΔT_d , are devoid of model bias. Therefore, new d_i are calculated from the monthly $T - T_d$ distribution at Changins and Δ are added on those new classes.

In order to verify the validity of the method, monthly Δ are added to the current data generated by the HIRHAM model (i.e., 1961–1990)

Table 3. Monthly differences between HIRHAM RCM future and current data.

Month	S_{\downarrow} ($W\ m^{-2}$)	C	T (°C)	T_d (°C)	v at 10 m ($m\ s^{-1}$)
January	-9.68	0.06	4.12	3.00	0.127
February	-17.05	0.1	2.97	2.70	0.066
March	-20.37	0.07	1.71	2.24	0.057
April	0.48	-0.03	3.03	2.78	-0.041
May	19.80	-0.06	3.50	2.83	0.008
June	26.10	-0.09	4.18	2.96	-0.003
July	13.04	-0.07	4.52	2.18	0.037
August	26.38	-0.12	6.87	1.26	0.030
September	16.03	-0.08	6.03	1.57	-0.050
October	-0.39	-0.02	4.50	2.88	-0.030
November	6.75	-0.05	4.02	0.86	-0.087
December	-3.00	0.01	4.12	2.18	0.043

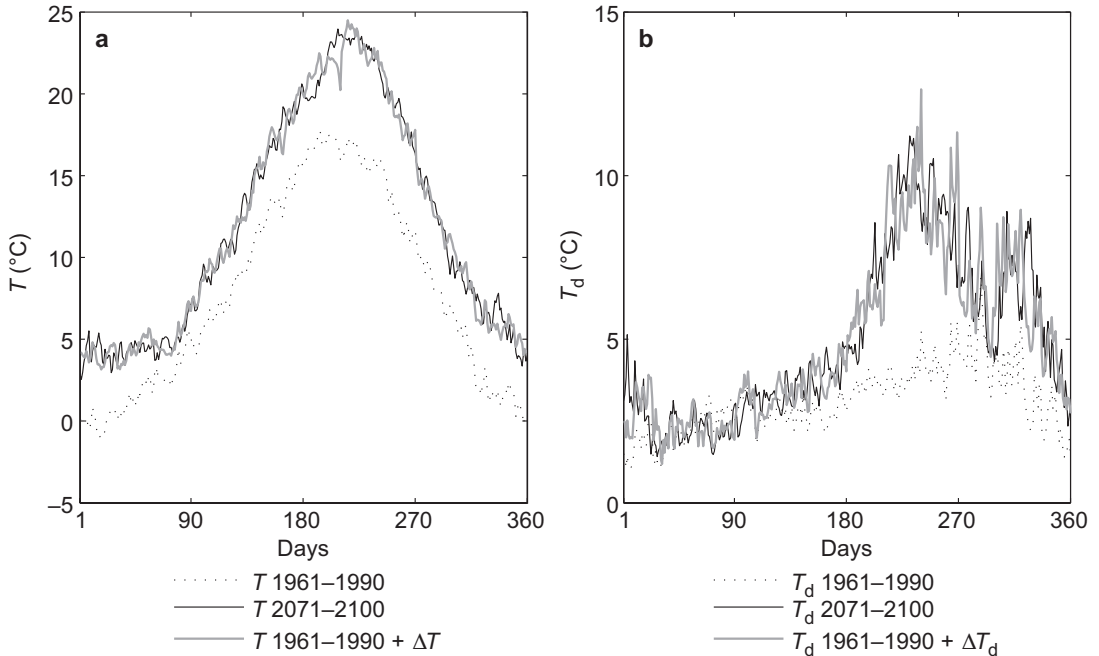


Fig. 7. Mean daily distribution of (a) temperature and (b) dew point temperature according to the HIRHAM outputs for the current and future period, as well as when monthly Δ are added to HIRHAM current data.

and the new distribution compared with the one predicted for the future (i.e., 2071–2100). It is shown that $T + \Delta T$ (ΔT being Δ for T) and $T_d + \Delta T_d$ (ΔT_d being Δ for T_d) are quite similar with the expected values at any time of the year (Fig. 7a and b). ΔT indicate that greatest warming is observed for maxima of T ($> d_0$) from April to October and for minima from December to March ($< d_1$). Overall, ΔT is more pronounced in summer than in winter. ΔT in the median class (between d_5 and d_0) is 6.79 °C in August whereas it reaches only 4.13 °C in January. Even though predictions for both T and T_d point out a shift in the distribution towards higher values, these variables will not evolve in the same manner. Therefore, it is likely that difference between T and T_d increases further due to a lower augmentation of T_d , thus impacting on RH; this is true for the whole year except for March. Changes concern mainly July, August and September (e.g. high difference at Julian day 180, Fig. 7a and b) where the decrease of RH reaches 15% on average during this period, in line with the findings of Christensen and Christensen (2003). ΔT_d above d_5 are also expected to be the largest. This means that reduction in RH will be observed

principally for dry atmospheric conditions but that the number of days close to saturation will not necessarily decrease.

Experimental setup

To simulate the evolution of Lake Geneva temperature profiles well beyond the observation period, a pseudo-random meteorological data generator is used to reproduce a 130-year sequence of meteorological data representative of the conditions recorded between 1961 and 1990. According to the amplitude of climate change simulated by the HIRHAM RCM, another dataset is produced by perturbing this long time-series according to Eq. 2. The first 10 years serve to spin up the water temperatures ($\lambda = 0$, i.e., no perturbation is applied) and the following 110 years to reproduce the evolution of the climate from the present to the future. In the following, λ is equal to 0 in 1976 (median year for the first period) and increases linearly up to 1 in 2086 (median year for the second period), followed by extra 10 years using a fixed $\lambda = 1$ in order for a new equilibrium to be reached

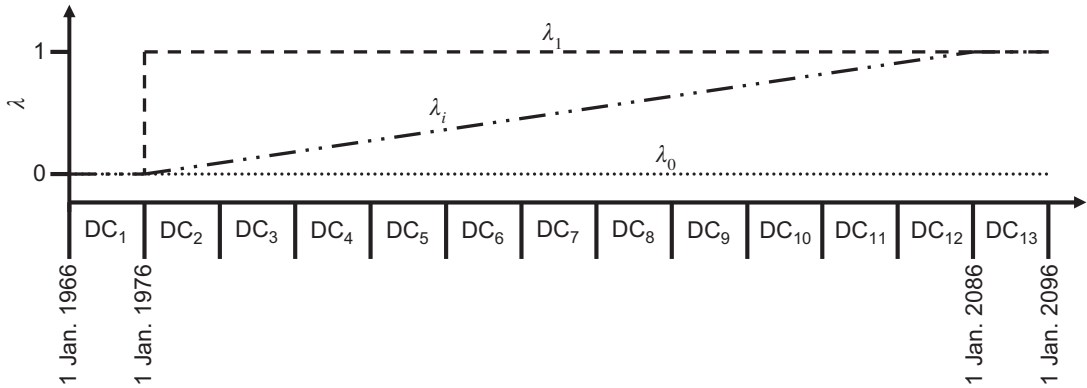


Fig. 8. Possible yearly values taken by the empirical scaling parameter λ to perturb the reference dataset over the 13 decades of simulation.

(Fig. 8). A number of simulations are then run with current (reference simulation) and future conditions over this long period. Daily water temperature profiles produced during the last decade are averaged daily to produce 365 profiles and serve to estimate the changes.

The thermal response of the lake to a constant λ ($\lambda = 1$ from year 11 to year 130) is also investigated for comparison since many studies concerned with climatic effects on lakes usually perturb historical weather recorded data with a unique and constant value (Fig. 8). This will provide a quantification of the time spent to reach the second equilibrium. Hereinafter, λ is referred to as λ_0 when λ is equal to zero (reference simulation), as λ_i when λ is increasing over the period, and as λ_1 when λ is held constant and equal to 1 (Fig. 8).

Since no coupled-biochemical model is used, existing measurements of K_c serve to produce daily values. However, in order to dampen the effects of high eutrophic status measured prior to 1990 on the absorption of solar radiation by the lake water, daily K_c have been averaged for similar Julian days over a period that covers the years 1981 to 2006. Water temperature variability resulting from fixed average values in K_c is then discussed below.

Changes in water temperature profiles are investigated in terms of volume-weighted temperatures in the epilimnion T_{epi} and in the hypolimnion T_{hyp} . The epi-hypolimnion boundary z_{lim} is then set at the depth z corresponding to the highest water temperature gradient (for a

layer spacing of 1 m). As z_{lim} evolves dynamically, the depth of the thermocline is defined as the average value of z_{lim} over the summer-autumn stratification period (Hambright *et al.* 1994). The onset of the stratification, OS, as well as the stability of the water column (given by the stability parameter, N^2) at z_{lim} , are considered with regard to their potential influence on biological processes. OS is diagnosed when a 1 °C difference appears between the 100 m and 2 m layers (adapted from Jacquet *et al.* 2005 and detailed in Perroud *et al.* 2009).

Surface energy exchanges and the resulting budgets are also computed (Table 1) since they determine the cooling/heating of the water body due to climatic forcings.

Results

Water temperatures profiles have been produced with SIMSTRAT driven by a 130-year pseudo-random hourly series. These results will allow to quantify changes due to global warming as compared with the reference simulation. As shown previously with the 100-year simulation (Fig. 6), mean decadal temperature profiles are reproduced in a realistic manner over the decades and simulate profile statistics similar to these obtained by using observations (1981–1990) (Fig. 5). At the bottom, mean water temperature is of 5.33 °C by the 13th decade. From the bottom up to the 100 m depth, mean decadal temperatures increase but do not exceed 0.2 °C.

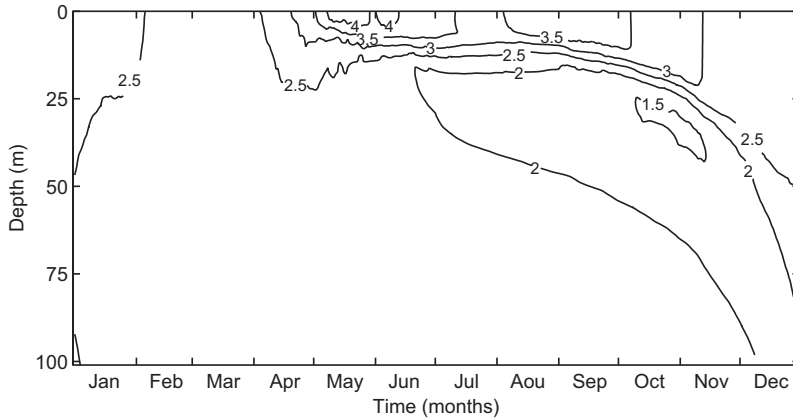


Fig. 9. Plots of mean daily temperature differences in the first 100 m below the surface between simulated profiles beyond the 13th decade under future and current conditions.

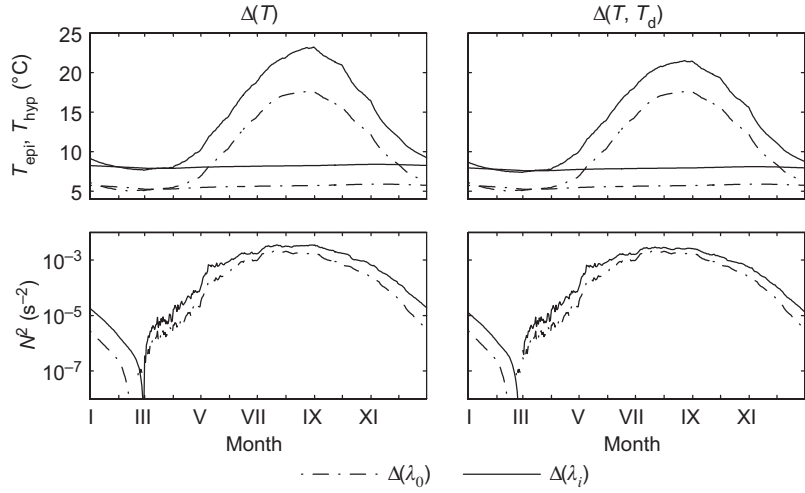
It is mainly above 100 m that changes are the most significant, particularly above 50 m. Temperatures are thus 6.10 °C at 50 m, 7 °C at 30 m, 10.3 °C at 10 m and 11 °C at the surface. T_{epi} is the highest in August where it reaches 17.45 °C and the lowest in February (5.09 °C). T_{hyp} is between 5.25 °C (March) and 5.88 °C (November), thus showing the shift in the cooling (heating) of the hypolimnion.

Projected Lake water temperature changes using the decile method

Two simulations driven by perturbed data based on a linear increase of the atmospheric perturbation were run. In the first, monthly perturbations were applied only to temperature (Sim_T) and in the second to temperature and relative humidity ($\text{Sim}_{T,RH}$). In both cases, an increase in water temperature was simulated in the entire water column. The annual temperature increase from the 35-m depth down to the bottom vary between 2.35 °C and 2.57 °C in case of Sim_T and between 2.10 °C and 2.28 °C in case of $\text{Sim}_{T,RH}$. Temperatures then rise strongly from 35 m up to the surface, so the increase is 2.54 °C (Sim_T) and 2.27 °C ($\text{Sim}_{T,RH}$) at 20 m, 3.31 °C (Sim_T) and 2.83 °C ($\text{Sim}_{T,RH}$) at 10 m, and 3.9 °C (Sim_T) and 3.16 °C ($\text{Sim}_{T,RH}$) at the surface. Intrannual variability indicates that during the winter months, warming through the column is between 2.37 °C and 2.93 °C for Sim_T , and between 2.11 °C and 2.72 °C for $\text{Sim}_{T,RH}$. Then, after the onset of the stratification, the lake can be partitioned into three segments with distinct warming trends: the

surface layers are expected to warm the most, the metalimnic layers below the thermocline the least, and the temperature in the hypolimnion to rise to values similar to those observed prior to stratification (Fig. 9). As heat entering the lake is not homogeneously mixed above z_{lim} , variability in water temperature may be important (Fig. 9). In the epilimnion, warming varies between 2.80 °C and 6.07 °C for Sim_T , and 2.40 °C and 4.17 °C for $\text{Sim}_{T,RH}$, the highest temperature increase being simulated at shallower depths, and mostly from early August to late September for Sim_T (> 5 °C), and from mid-May to mid-June for $\text{Sim}_{T,RH}$ (> 4 °C). As compared with the values simulated at the depth of the lower metalimnion before stratification, water temperatures increase. However, Sim_T and $\text{Sim}_{T,RH}$ show that warming below the thermal gradient will be lower than further down in the column, and particularly from early July (Fig. 9). These layers evolve dynamically downwards with a deepening of the thermocline. A minima of 1.59 °C for Sim_T and 1.62 °C for $\text{Sim}_{T,RH}$ are thus found at 18 m and 23 m, respectively, in early September. From the bottom up to this limit, daily variability in the thermal increase is 2.42–2.63 °C for Sim_T and 2.15–2.33 °C for $\text{Sim}_{T,RH}$. This indicates that predictions for Sim_T impact more strongly water temperatures than those for $\text{Sim}_{T,RH}$ (Fig. 10). Similarly, the monthly increase of T_{epi} was between 2.58 °C (March) and 5.35 °C (August) for Sim_T , whereas the increase ranged from 2.32 °C and 3.83 °C for $\text{Sim}_{T,RH}$. Likewise, monthly T_{hyp} rose by 2.50–2.63 °C for Sim_T and by 2.20–2.33 °C for $\text{Sim}_{T,RH}$. A T_{epi} slightly lower or similar to T_{hyp} (≤ 0.3 °C) simulated under cur-

Fig. 10. Mean daily volume-weighted temperatures in the epilimnion T_{epi} and hypolimnion T_{hyp} , for SIMSTRAT simulations under present and future conditions, when T and both T and T_d are perturbed (upper row). Similar results are shown for daily values of water column stability, N^2 (lower row).



rent conditions from January to March was also observed under both future projections, but only in February and March (≤ 0.2 °C).

The main changes in the metalimnic properties concerned the overall greater stability of the lake. In future, N^2 is 3 times greater in spring, (Fig. 10) and 1.5 times greater in summer. During summers, z_{lim} generally agrees under current and future conditions, but in future the thermocline depth in autumn moves closer to the surface (2–4 m upwards on average), thus indicating a longer period of stratification (up to 11 days more). Moreover, the lake will stratify earlier, on average little more than one week, so that the length of the stratification period will be more than 3 weeks longer than under current climate.

The total daily energy amount for each flux component was averaged per decade in order to analyse the differences observed in the water column between both perturbed simulations and to diagnose the amount of heat gain or loss by the lake (Fig. 11). Air temperature dependent fluxes, $L\downarrow$, Q_h , Q_e , are analysed since they strongly affect the lake surface energy budget, and thus the amount of heat available to warm the lake water column. However, omitting the decrease in RH, the atmospheric emissivity, ϵ_a , is overestimated, producing higher values of $L\downarrow$ (Table 4). Reduction in water vapour, e_a , (Table 1) following drying of the atmosphere, jointly with surface water temperature changes, is seen to cool the water by evaporation more intensively than in Sim_T alone (Table 4).

At the same time when perturbations linearly increase in Sim_T and $Sim_{T,RH}$, it appears that $L\downarrow$ increases under the new climatic conditions at a mean rate of 0.21 (Sim_T) and 0.17 ($Sim_{T,RH}$) MJ day⁻¹ m⁻² per decade. The other fluxes, whose values also depend on the lake surface temperature, remained negative on an annual average basis. Due to higher surface water temperature, there were additional 0.14 (Sim_T) and 0.11 ($Sim_{T,RH}$) MJ day⁻¹ m⁻² that were extracted by the loss of infrared energy. In addition, negative values of Q_e further cooled the lake at a mean rate of 0.07 (Sim_T) and 0.09 ($Sim_{T,RH}$) MJ day⁻¹ m⁻². Even though Q_h is still negative, the amount of energy lost from this latter component were decreasing at a mean rate of 0.015 (Sim_T) and 0.049 ($Sim_{T,RH}$) MJ day⁻¹ m⁻². As compared with

Table 4. Mean energy components calculated over the 13th decade of simulation under current (reference simulation) and future conditions (Sim_T , $Sim_{T,RH}$).

Fluxes (MJ day ⁻¹ m ⁻²)	Reference simulation (LDP)	Sim_T	$Sim_{T,RH}$
$S\downarrow$	11.97	11.97	11.97
$S\uparrow$	0.88	0.88	0.88
S^*	11.95	11.09	11.09
$L\downarrow$	24.93	27.54	27.01
$L\uparrow$	-31.30	-32.97	-32.54
L^*	-6.24	-5.43	-5.61
Q_h	-0.73	-0.56	-0.17
Q_e	-4.11	-5.12	-5.34
Energy budget	-0.02	-0.03	-0.04

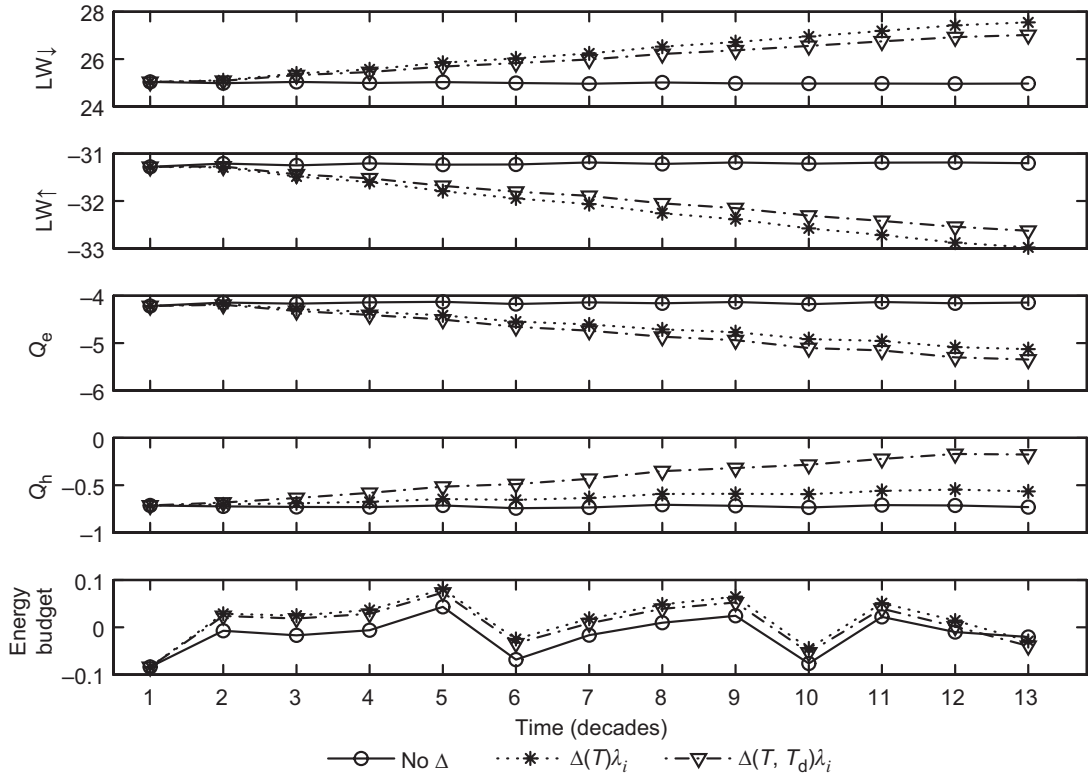


Fig. 11. Total daily energy amount for L_{\downarrow} and L_{\uparrow} , infrared gain or loss at the lake surface, Q_e , latent heat flux, Q_h , sensible heat flux and total energy budget, averaged per decade for the reference simulation and for both perturbed simulations Sim_T , $Sim_{T,RH}$. Units are in $MJ\ day^{-1}\ m^{-2}$.

the reference simulation, the energy budget indicated that the mean multi-decadal energetic gain is 0.036 and $0.027\ MJ\ day^{-1}\ m^{-2}$ for Sim_T and $Sim_{T,RH}$, respectively.

Sensitivity of the lake water temperature to changes in air temperature.

Two additional simulations have been undertaken with a bulk increase of $1\ ^\circ C$ (Sim_{T1}) and $4\ ^\circ C$ (Sim_{T4}) in air temperature. The lake response to various increases in air temperature will allow to conclude whether nonlinearities appear in the system. In any case, an increase of $1\ ^\circ C$ or more produces a warming of the entire water column over the year. Seasonal variability of changes in the water temperature profile is 0.6 – $0.68\ ^\circ C$ below $75\ m$ (Sim_{T1}) and 2.73 – $2.95\ ^\circ C$ (Sim_{T4}) below $85\ m$. From that limit up to the surface, changes for Sim_{T1} and Sim_{T4} are higher and reach

respectively the maxima of $0.75\ ^\circ C$ and 3.16 in winter, $0.98\ ^\circ C$ and $4\ ^\circ C$ in spring, $1.06\ ^\circ C$ and $4.05\ ^\circ C$ in summer and $0.90\ ^\circ C$ and $3.60\ ^\circ C$ in autumn. As for $Sim_{T,RH}$, weaker changes appear in the area situated below the thermocline in summer and autumn, with the minima of $0.52\ ^\circ C$ (Sim_{T1}) and $2.35\ ^\circ C$ (Sim_{T4}). Warming of the water due to an increase of $1\ ^\circ C$ or $4\ ^\circ C$ in air temperature produces seasonal ratios through the column that range from 3.8 to 4.6 . Smallest ratios are found above the thermocline. Furthermore, it is during summer and autumn that the values lower than 4 were calculated, i.e., in the first $10\ m$ (Sim_{T1}) and $8\ m$ (Sim_{T4}) below the surface. During these stratified periods, the highest ratio (> 4.4) are found in the metalimnion.

The monthly increase in T_{epi} varies between $0.70\ ^\circ C$ (February) and $1.26\ ^\circ C$ (March) for Sim_{T1} and between $3.01\ ^\circ C$ (February) and $4.23\ ^\circ C$ (July) for Sim_{T4} . Similarly, changes in T_{hyp} , with respect to the increase in air tem-

perature, are 0.64–0.69 °C and 2.81–2.97 °C for Sim_{T_1} and Sim_{T_4} , respectively.

Variability of light extinction coefficient on lake water temperature

The sensitivity of the light extinction coefficient on the thermal profiles has been tested for $Sim_{T_{RH}}$ by varying K_e in the range of $\pm 25\%$. Deeper penetration of S_{\downarrow} in the lake, followed by a reduction of K_e , increased water temperature with depth and reduced it at the surface. However, changes in water temperature through the profile for a low K_e (-25%) are significant only above 30 m and for all seasons except for winters. Below 30 m and in winter, mean temperatures change (compared with the reference simulation) by less than 0.1 °C. In spring, summer and autumn, the highest temperature increase with depth is simulated at 12 m (0.09 °C), at 11 m (0.81 °C) and 16 m (0.64 °C). The decrease in near-surface temperature is mainly observed in spring and summer and affects the first 5–6 m below the surface (-0.14 °C and -0.26 °C at the most in spring and summer, respectively). A maximum decrease of 0.49 °C is simulated at the surface in August. In autumn, temperatures are even warmer in the surface layers, probably due to mixing processes appearing between the hypolimnetic (warmer with respect to the reference simulation) and epilimnetic layers. On the contrary, near-surface water temperatures increase at the expense of deeper layers when K_e increases. Again, variations of water temperature are observed only in the first 25 m of the profile and in summer and autumn. Outside those periods, seasonal changes are less than 0.05 °C. The strongest decrease in temperature (-0.86 °C) is simulated at 9 m in summer and at 14 m in autumn (-0.34 °C). The temperature increase observed in the near-surface water reaches 0.22 °C at maximum (surface layer). A daily-average temperature increase exceeds occasionally 0.7 °C in August.

Variability in T_{epi} is balanced by the fact that z_{lim} lie much deeper than the increase (-25% K_e) or decrease (-25% K_e) in near-surface temperature. Depending on K_e variability, the maximum monthly differences between simulations with

maximum range of variation ($\pm 25\%$) are 0.33 °C in T_{epi} and 0.05 °C in T_{hyp} .

Variability of wind speed on lake water temperature

According to the IPCC A2 scenario, changes in wind speed, as simulated by HIRHAM, are expected to be small in future. The mean annual difference is 0.01 m s⁻¹ and no notable bias appears through the months (Table 3). Since Δv isn't large, the decile method could not be applied to this variable. However, sensitivity of water temperature profiles to variations of $\pm 20\%$ of v has been tested for $Sim_{T_{RH}}$.

Under stronger wind conditions, the onset of the stratification is delayed (by 1 week on average) and, once established, strength of the stratification is weaker ($1.5 \times$ in summer) and the thermocline is lowered on average by 3 m. As compared with $Sim_{T_{RH}}$, the profiles are warmer, except in the upper layers in spring, summer and autumn. The additional increase in the seasonal temperature profiles varies between 0.6 °C and 0.86 °C in winter, and rises to 0.67 °C (45 m) in spring, 1.9 °C (20 m) in summer and 2 °C (30 m) in autumn. In the upper layers, the cooling is particularly important in summer (-0.98 °C) and autumn (-0.21 °C). The downward shift of the thermocline from the onset to the destratification is larger than in $Sim_{T_{RH}}$. It is 1 m deeper than in $Sim_{T_{RH}}$ in summer and 7 m in autumn.

Weaker winds produce an opposite effect. The thermocline is thus established earlier (1 week) and the stratification becomes stronger ($1.5 \times$ in summer). Less wind leads to a thermocline on average 3 m closer to the surface than in $Sim_{T_{RH}}$ and to a reduction of heat penetration. As compared with $Sim_{T_{RH}}$, this latter leads to an overall cooling of the water temperature profile. Negative changes lie within 0.71 °C and 1 °C in winter or vary between no difference (where the thermoclines meet) and 0.26 °C in spring (36 m), 2.3 °C in summer (16 m) and 2.5 °C in autumn (24 m). The downward movement of the thermocline is very smooth and the temperature gradient lasts longer. The thermocline is located 1 m shallower than in $Sim_{T_{RH}}$ in summer and

5 m in autumn. Heat that accumulates in the upper layers during the stratified period warms the water up to 0.26 °C, 0.89 °C and 0.25 °C in spring, summer and autumn, respectively.

A 20% increase of the wind speed in Sim_{T,RH} cools T_{epi} only during the stratified months and inversely following a reduction of the wind speed. Thus T_{epi} may decrease by 0.02 °C (April) to 1.12 °C (July) or increase by 0.24 °C (October) to 1.06 °C (July). During the coldest months, due to missing or low stratification, T_{epi} evolves with respect to T_{hyp} . Variability of T_{hyp} ranges between 0.6 °C and 0.75 °C for higher wind speed and 0.7 °C and 0.84 °C for lower wind speed.

Variability of cloud cover on lake water temperature

Cloud cover changes expected in the future are small ($\Delta \bar{C} < 0.02$). The trend shows a slight increase in C during the winter months and a clearer sky during the rest of the year. Similarly, as for ν , variations were not sufficiently large to allow the decile method to be applied. Sensitivity to variations of C was assessed by running Sim_{T,RH} with the C variable increased and then decreased by 10%. The lake temperatures did not vary significantly in changes up to 10%. As compared with Sim_{T,RH}, an increase or a decrease of the C warmed or cooled the water by 0.14–0.17 °C or 0.13–0.16 °C, respectively from 18 m down to the bottom. Variability increased in the upper layer: the largest changes were observed at the surface in spring (+0.22 °C/–0.20 °C) and the smallest in autumn (+0.14 °C/–0.12 °C).

Changes evolve symmetrically in T_{epi} and in T_{hyp} with respect to the increase and decrease of C . Thus, the monthly amplitude went from 0.24 °C (September) to 0.42 °C (May) in T_{epi} and was equal to 0.30 °C in T_{hyp} .

The decile method with a linear increase vs. a constant Δ

The effects of a constant increase of atmospheric perturbations on the simulated water temperatures were estimated when both the temperature and relative humidity (Sim_{T,RH,1}) were allowed to

change. Simulated profiles with λ_1 (Fig. 8) were averaged per decade at each depth to produce 13 decadal profiles. Each decadal profiles DP_i ($i = [1, \dots, 13]$) obtained using λ_1 were compared with the last decadal mean profile simulated with λ_i (LDP). Water temperature from Sim_{T,RH,1} rapidly increased during the simulation, so that the maximum water temperature difference between DP_2 and LDP (Fig. 12) was of only 0.8 °C. Then, the difference between both DP_3 and DP_4 and LDP became even smaller. However, compared with the LDP, water temperatures were slightly overestimated above 13 m and 80 m, respectively, and still underestimated below. From DP_5 , values at each depth fluctuated around those averaged in the LDP and the mean error to the LDP was -0.039 ± 0.06 °C at the depth where the maximum difference occurs, i.e., 12 m. The lake may thus be considered as evolving towards a mean steady state after the fourth decade following the perturbation. As a consequence of the constant temperature change during the second decade, the mean lake energy budget became highly positive, 0.41 MJ day⁻¹ m⁻², and then fluctuated around zero on average. As compared with the reference simulation, there is even a mean energy loss of 0.0279 MJ day⁻¹ m⁻² from DP_3 to DP_{12} . Simulations with λ_1 are almost identical to LDP during the last decade where the same values are driving the model. A maximum difference of 0.019 °C is recorded at the bottom whereas the minimum (0.02 °C) is observed at the surface.

Discussion

The pseudo-random weather generator is a useful tool to drive the lake model in order to investigate the evolution of water temperature over periods that are longer than historical meteorological records. Moreover, the similarity between water temperature profiles produced by the reference simulation over decades shows that the generator is able to reproduce long and realistic datasets.

The decile method that has been applied to perturb the pseudo-random series used to drive the SIMSTRAT lake model indicates that warming of the thermal profiles is likely to occur,

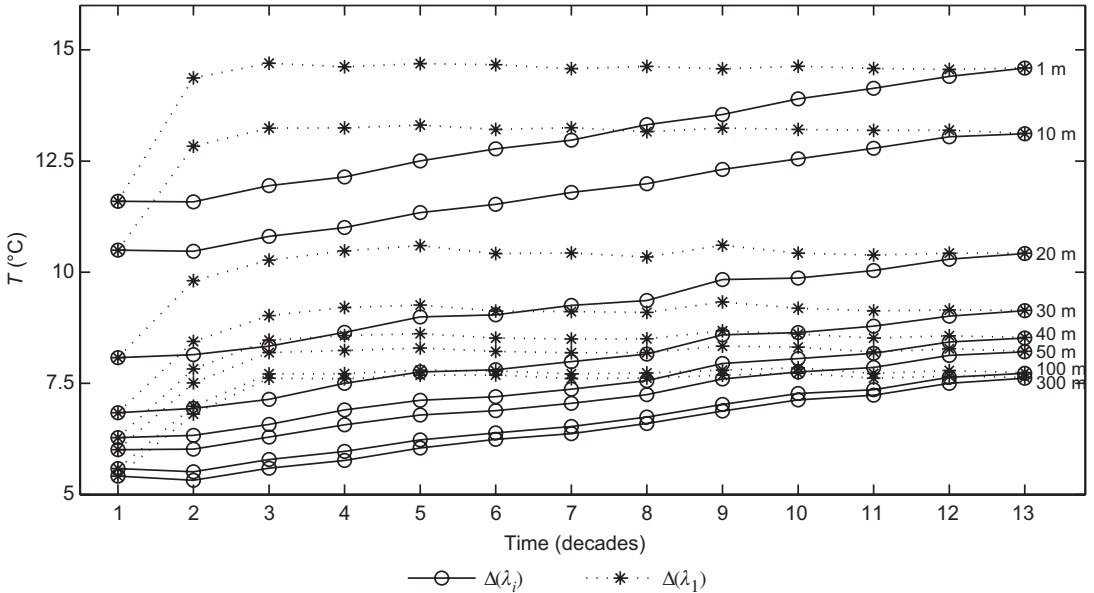


Fig. 12. Mean decadal temperature profiles obtained from the 130-year perturbed simulations $\text{Sim}_{T,\text{RH}}$ and $\text{Sim}_{T,\text{RH},1}$.

whether T or both T and RH are used. As compared with the reference simulation, a run using modified conditions warms the whole water column. This is caused by an increase in the surface longwave budget L^* and a decrease in heat lost by sensible heat Q_h . The cooling by stronger evaporation cannot compensate the positive flux towards the lake, thus producing a mean energy gain of $0.036 \text{ MJ day}^{-1} \text{ m}^{-2}$ (Δ applied to T) and $0.027 \text{ MJ day}^{-1} \text{ m}^{-2}$ (Δ applied to T and RH) over the 110-year period. However, changes in surface water temperature induced by the reduction of RH, as predicted by the HIRHAM model under future condition at the grid point over Lake Geneva, were significantly different from Sim_T outputs, leading to a decrease in water temperatures. Comparison of water temperature profiles from Sim_T and $\text{Sim}_{T,\text{RH}}$ revealed differences at all depths, particularly important in T_{epi} where it may reach $1.5 \text{ }^\circ\text{C}$ in August. The cooling that follows this decrease in RH is caused by a reduction of L^* as well as by an increase in the loss of heat by evaporation. Interestingly enough, an increase in surface temperature according to Sim_T leads to less evaporation than a simulation producing lower water surface temperature. This is due to a smaller water vapour deficit at the air–lake interface in Sim_T , indicating that changes induced by a decrease in RH have a

larger impact on the rate of evaporation than the increase in surface temperature only. The way the energy exchanges at the lake–atmosphere interface are affected by changes in saturation properties of air reveals the need to include this component in the simulations. A shift appears between the months during which data were most severely modified with respect to drier conditions and the maximum differences simulated in T_{epi} , i.e., one month on average. Therefore, the perturbation specified on a monthly basis seems to be a crucial component and should not be omitted when seasonal and monthly variability is concerned.

It has been shown that the sensitivity in daily profiles to the values of K_c ($\pm 25\%$) in the future is only notable at certain depths. The seasonal increase ($+25\% K_c$) vs. decrease ($-25\% K_c$) in near-surface layers water temperature produce changes generally below $0.25 \text{ }^\circ\text{C}$. Also, seasonal variations in water temperature below 30 m are in any case below $0.1 \text{ }^\circ\text{C}$. At some depths above 30 m, the largest changes are simulated in the range of $\pm 0.9 \text{ }^\circ\text{C}$ for summer and between $-0.34 \text{ }^\circ\text{C}$ ($+25\% K_c$) and $0.64 \text{ }^\circ\text{C}$ ($-25\% K_c$) for autumn. In reality, these high differences result from changes in the depth of the thermocline (deeper when K_c is reduced) and not from strong variations in the water temperature profiles.

Monthly changes lie within 0.2 °C for T_{epi} and 0.05 °C for T_{hyp} . Therefore T_{epi} and T_{hyp} would remain essentially unchanged even though K_c vary within those limits in the future.

HIRHAM outputs indicate that T and T_d are expected to change in the future according to the IPCC A2 warming scenario. However, the sensitivity performed with the other driving variables, ν and C , show that the response of the lake would be significantly different. Actually, changes would concern only ν . In effect, sensitivity of Lake Geneva to variations in C ($\pm 10\%$) implies monthly changes smaller than 0.22 °C in T_{epi} and 0.16 °C in T_{hyp} . The largest seasonal change, observed at the surface is only 0.22 °C. On the contrary, variations of ν may induce seasonal changes of at least 0.6 °C through the column under unstratified conditions and changes reaching up to 2 °C below the thermocline during the stratified period. At the surface, where temperature changes are inverted as compared with those below the thermocline, differences may be larger than 0.89 °C. The evolution of the lake waters is strongly related to the behaviour of the thermocline. In fact, a 20% increase in ν is sufficient to delay the formation of the thermocline and weaken the stratification in Lake Geneva. As a consequence, surface waters heated in spring mix easily with deeper waters, thereby warming deeper layers of the column at the expense of the surface waters, and fostering the development of a deep thermocline, 3 m deeper than current. This latter also helps to explain the large shift in temperatures observed in summer and autumn. During the stratified period, less stability also eases heat exchanges between the epilimnion and the hypolimnion, providing heat to deeper layers. A reduction of 20% in ν would imply reverse processes, and thermal effects of the same order. Large monthly amplitudes in T_{epi} (2.18 °C) and T_{hyp} (1.60 °C) resulting from $\pm 20\%$ change of ν emphasize the need to be careful when assessing the impact of climate change on such a large water body.

$\text{Sim}_{\text{T,RH}}$ produces a strong increase in T_{epi} that lies generally below that of the air temperatures, given by the smallest monthly ΔT . However, one exception is observed in March when the increase in T_{epi} exceeds the increase in air temperature of the 9th highest value of monthly

ΔT . This suggests that even though ΔT 's are the smallest during this month for all classes and shift in T_{epi} the lowest, the mixing of epilimnic water with part of hypolimnic water volume as well as the short duration of colder conditions prevent intensive cooling of surface waters, keeping the entire water column close to mean hypolimnic temperatures. The shift in surface water temperatures during the coldest periods is then related more to minimum monthly T_{hyp} than to the increase in air temperature. The monthly increases in T_{epi} simulated in this study are slightly less than the average annual increase in the air temperature (3.9 °C) and, with the exception of March, represent 55%–98% of the increase in monthly mean air temperature. From mid-May to mid-June, water surface temperatures may even exceed the average annual air temperature increase. This conclusion is in close agreement with the results of many studies that found greater increase in air temperature than in epilimnic temperature (Hondzo and Stefan 1993, Stefan *et al.* 1993, DeStasio *et al.* 1996, Peeters *et al.* 2002, Peeters *et al.* 2007). Similar predictions have resulted in similar conclusions for Lake Constance, located between Switzerland and Germany (Peeters *et al.* 2007): epilimnic temperatures are only slightly lower than the fixed increase of 4 °C that perturbed a long time-series of observed data whereas the increase observed in April may even exceed this threshold. However, monthly maximum increases in the epilimnic temperatures are not predicted to take place at the same time in Lake Constance (April) and Lake Geneva (August). Since the highest perturbations are applied in August to Lake Geneva, it is likely that those differences arise from the monthly ΔT used.

Unlike earlier studies (Robertson and Ragotzkie 1990, Hondzo and Stefan 1991, DeStasio *et al.* 1996, Stefan *et al.* 1998) that predicted a slight increase in the bottom water temperatures and in some cases, even a decrease, simulations of Lake Geneva temperature profiles indicate that the warming may be strong and even exceed 2.3 °C in T_{hyp} . This finding is similar to results predicted for other perialpine deep lakes, such as Lake Constance (Peeters *et al.* 2007) and Lake Zurich (Peeters *et al.* 2002). In those lakes, a fixed 4 °C increment to air temperature records

raised the hypolimnion temperatures in all seasons inducing a mean difference exceeding 2 °C in Lake Constance and 1.4 °C in Lake Zurich. In order to explain this trend that is observed in monomictic lakes, Peeters *et al.* (2002) assumed that complete mixing that may potentially occur in future will not cool the bottom temperature of monomictic lakes to values lower than the minimum epilimnic temperatures. Since the minimum epilimnic temperatures are expected to increase, hypolimnic temperatures will also increase in accordance with the trend observed during the coldest part of the year.

Lake stability was studied by many authors with respect to perturbations for example in air temperature and wind speed (Hondzo and Stefan 1991, 1993, DeStasio 1996, Stefan *et al.* 1998). These studies generally agree that a more intense stratification will take place. Consistency with those assumptions is found in Lake Geneva, since the warming of the whole water column is stronger for T_{epi} than for T_{hyp} . Temperature difference may reach +0.88 °C. This hypothesis is reinforced by the higher N^2 values that have been calculated for the future conditions. As a consequence of this higher stability, the penetration of heat decreases. As a matter of fact, heat is stored in the upper layers and rises the temperatures of surface waters, thus leading to a differential warming of the water column (Fig. 9). Succession patterns of daily profiles highlights a lower metalimnion where the expected increase in water temperature was less important than the smallest changes observed in the hypolimnion. In fact, strenghtening of the stratification in the future may impact strongly on metalimnic properties. A higher stability may reduce epi-hypolimnic heat exchanges as compared with today's regime. This point may be relevant for species that would be more temperature dependent than stability or light penetration dependent. However, the persistence of T_{epi} in late winter below T_{hyp} under a warmer climate as well as a similar increase in epilimnic and hypolimnion temperatures in March suggests that overturns might still occur occasionally (Fig. 10), or at least as frequently as today. The period for which T_{epi} is smaller or equal to T_{hyp} is expected to be reduced, thus impacting the events of partial or complete turnover. Likewise, frequency of

complete mixing in some deep lakes (projected to become monomictic, if not already the case) is expected to decrease and the period of mixing to be of shorter duration (Croley 1994, Peeters *et al.* 2002).

Changes in the duration of summer stratification (> 3 weeks) match the predictions of many other authors (Robertson and Ragotzkie 1990, Boyce *et al.* 1993, Stefan *et al.* 1996, Stefan *et al.* 1998, King *et al.* 1999). In Lake Geneva, the increase in the period of stratification is almost equally due to changes in the start and end of stratification.

Sensitivity of Lake Geneva to a constant increase of air temperature, as deduced from Sim_{T_4} , may serve as a tool to evaluate what the more complex decile method has brought to the prediction of water thermal profiles. This assessment is possible since the mean annual temperature difference between the HIRHAM current and future data is 4 °C. The comparison between water temperature profiles simulated by Sim_{T_4} and Sim_T shows that the differences can largely be attributed to variabilities in ΔT . An increase of 4 °C is higher than any ΔT calculated by the decile method from February to April, and lower by at least the third smallest increment from July to October. As a result, Sim_{T_4} overestimates T_{epi} before the onset of stratification whereas the warming is much too low at the time of stratification (< 1.5 °C in August and September). Even though less heat accumulates in T_{epi} in summer, the lack of variability in ΔT in early spring contributes to the more intense warming of T_{hyp} (+0.3 °C) and to the reduction of the mixing period duration. Furthermore, sensitivity of Lake Geneva to various increases in air temperatures has shown that linearity in the thermal response of the lake exist. The ratio deduced from respective changes in water temperature due to an increase of 4 °C and 1 °C in air temperatures, is of 4.1 ± 0.3 , at any time and any depths, with the exception of the metalimnion. Here, the slight nonlinearities can be explained by the shallower position of the thermocline during the stratified month simulated for a 1 °C increase in air temperature. Even though the stratification is also weaker, the shallower thermal gradient reduces the depth of heat penetration. This analysis confirms the strong link

that exists between the increase in air and water temperatures and the need for including at least monthly variations.

Whether climate change is applied abruptly or progressively to atmospheric data driving the lake model, the resulting water temperature profiles as well as energy budgets are very similar. However, the data perturbed according to λ_1 provided during the first perturbed decade slightly more energy to the lake than the total amount added over the 11 decades when data are perturbed progressively. The overestimated temperatures in the upper waters and underestimated temperature in the lower waters for former decades indicate that the lake needs more than a decade to equal values of the LDP. The continuous multi-decadal energy loss thus reduces the high amount of energy obtained during the first perturbed decade (for the λ_1 simulation) over the following decades up to a steady state. Lake Geneva reacts quite rapidly to a change in weather conditions. For a lake as deep as Lake Geneva, at least four decades are required to reach a steady state. Impacts on the water temperature profiles of modified meteorological data produce realistic results from the fourth perturbed decade onwards. This is true even though it is only from the eight perturbed decade that the mean energetic balance equals the one of LDP. While the goal is to estimate the increase in water temperature by the end of the century, the insignificant bias between profiles obtained using λ_1 or λ_i (< 0.014 °C) reveals that both methods can be used as long as the simulation with λ_1 is run over a sufficiently long period.

Conclusion

This study has investigated the evolution of Lake Geneva water temperature profiles under conditions of global warming using the one-dimensional lake model SIMSTRAT. Long simulations are required to take heat storage into account in the deep hypolimnion and to accurately assess future water temperatures profiles. A 130-year simulation has thus been undertaken with variables representative of the current period and others perturbed according to expected changes in monthly distribution.

The statistical method used to produce meteorological datasets has been shown to represent a reasonable alternative when long-term historical records are missing. Moreover, this technique randomly produces extreme events or particular periods over the period and removes those that would appear spuriously if only observed data were used. During its development process, it has been shown that variability of the wind on the accuracy of simulated temperature profiles is essential.

The runs done over a large number of years allow to track the heat accumulation in the deep hypolimnion and to have a measure of confidence regarding the projected changes at the bottom. However, this study has shown that 40 years are required to stabilize the heat exchange at the lake–atmosphere interface and to obtain accurate temperature changes throughout the water column when a constant perturbation is applied to current data.

The decile method developed in this paper to reproduce future climate from RCM outputs superimposed on the observed data has proven genuine skill to drive the lake model. This method accounts not only for changes in the mean but also in the different parts of the probability density function, such as maxima and minima. It should be noted that changes presented here result from projections provided by the HIRHAM RCM only; the mean annual difference in temperature simulated by this RCM (3.9 °C at grid point over Lake Geneva) lies within the range of values defined by other RCMs for Europe under the A2 scenario (Déqué *et al.* 2005, Alcamo *et al.* 2007, Beniston *et al.* 2007). Therefore, the thermal response of the lake can be considered a good approximation of the mean increase projected by a set of RCMs.

The sensitivity of the water temperature profiles to the meteorological variables as drivers of climate change demonstrated the need to include more than just the temperature. The water temperature increases which result from the perturbation of T and RH are significant, exceeding 4 °C at the surface, and reaching 3.83 °C in the epilimnion and 2.33 °C in the hypolimnion.

It is likely that these increases will impact the ecosystem of Lake Geneva. Based on these findings, effects of climate change on various aspects of lake ecological systems should be investigated.

Among them, special attention should be paid to the frequency of occurrence of harmful algal blooms, such as the cyanobacteria *Planktothrix rubescens* that has been observed in Lake Geneva (Jacquet *et al.* 2005). As a result of higher temperatures, increased stability of the water column and reduction of the vertical turbulent mixing, lakes — particularly eutrophic lakes — are likely to be more regularly affected in the future by these toxic algae (Roelke and Buyukates 2002, Kanoshina *et al.* 2003, Jöhnk *et al.* 2008, Shatwell *et al.* 2008). Changes in vertical mixing within the water column related to thermal stratification are extremely important as they are usually accompanied by changes in the availability of nutrients and light (Anneville *et al.* 2005, Winder and Hunter 2008). Therefore, findings from this study could also suggest ways to assess the timing of the phytoplankton spring bloom, growth capacity of phytoplankton and changes in phytoplanktonic communities. To study the possible responses of aquatic ecosystems to a warmer climate, the complexity of processes and exchanges taking place through the water column also implies that a coupled ecological model needs to be used.

Acknowledgments: We would like to thank Martin Beniston for the helpful discussions, valuable suggestions in preparing this paper and also for proof-reading the manuscript. We also wish to thank the EU-PRUDENCE project for making the online data available. We also thank the reviewers for their comments on this manuscript.

References

- Alcamo J., Moreno J.M., Nováky B., Bindi M., Corobov R., Devoy R.J.N., Giannakopoulos C., Martin E., Olesen J.E. & Shvidenko A. 2007. Europe. In: Parry M.L., Canziani O.F., Palutikof J.P., van der Linden P.J. & Hanson C.E. (eds.), *Climate change 2007: impacts, adaptation and vulnerability*, Contribution of Working Group II to the Fourth Assessment Report of the Intergovernmental Panel on Climate Change, Cambridge University Press, Cambridge, pp. 541–580.
- Anneville O., Gammeter S. & Straile D. 2005. Phosphorus decrease and climate variability: mediators of synchrony in phytoplankton changes among European peri-alpine lakes. *Freshwater Biol.* 50: 1731–1746.
- Bantle H. 1989. *Programmdokumentation Klima-Datenbank am RZ-ETH Zürich*. MeteoSwiss Publication, Zürich.
- Beniston M., Stephenson D.B., Christensen O.B., Ferro C.A.T., Frei C., Goyette S., Halsnaes K., Holt T., Jylhä K., Koffi B., Palutikoff J., Schöll R., Semmler T. & Woth K. 2007. Future extreme events in European climate; an exploration of Regional Climate Model projections. *Clim. Change* 81: 71–95.
- Bennett J.R. 1978. A three-dimensional model of Lake Ontario's summer circulation: II. A diagnostic study. *J. Phys. Oceanogr.* 8: 1095–1103.
- Burchard H. & Baumert H. 1995. On the performance of a mixed layer model based on the $k-\epsilon$ turbulence closure. *J. Geophys. Res.* 100: 8523–8540.
- Boyce F.M., Hamblin P.F., Harvey L.D., Schertzer W.M. & McCrimmon R.C. 1993. Response of the thermal structure of Lake Ontario to deep cooling water withdrawals and to global warming. *J. Great Lakes Res.* 19: 603–616.
- Christensen J.H. & Christensen O.B. 2003. Severe summertime flooding in Europe. *Nature* 421: 805–806.
- Christensen O.B., Christensen J.H., Machenhauer B. & Botzet M. 1998. Very high-resolution regional climate simulations over Scandinavia — present climate. *J. Climate* 11: 3204–3229.
- Coats R., Perez-Losada J., Schladow G., Richards R. & Goldman C. 2006. The warming of Lake Tahoe. *Clim. Change* 76: 121–148.
- Croley T.E. 1994. Hydrological impacts of climate change on the Laurentian Great Lakes. *Trends in Hydrology* 1: 1–25.
- De Stasio B.T., Hill D.K., Kleinhans J.M., Nibbelink N.P. & Magnuson J.J. 1996. Potential effects of global climate change on small north-temperate lakes: physics, fish & plankton. *Limnol. Oceanogr.* 41: 1136–1149.
- Déqué M., Jones R.G., Wild M., Giorgi F., Christensen J.H., Hassell D.C., Vidale P.L., Rockel B., Jacob D., Kjellström E., de Castro M., Kucharski F. & van den Hurk B. 2005. Global high resolution versus Limited Area Model climate change projections over Europe: quantifying confidence level from PRUDENCE results. *Clim. Dynam.* 25: 653–670.
- Dokulil M.T., Jagsch A., George G.D., Anneville O., Jankowski T., Wahl B., Lenhart B., Blenckner T. & Teubner K. 2006. Twenty years of spatially coherent deepwater warming in lakes across Europe related to the North Atlantic Oscillation. *Limnol. Oceanogr.* 51: 2787–2793.
- Fang X. & Stefan H.G. 1996. *Projections of potential climate change effects on water temperature, dissolved oxygen and associated fish habitat in small lakes of the contiguous U.S., vol. 1: Effects of past climate conditions*. Project Report 393. St. Anthony Falls Laboratory, University of Minnesota, Minneapolis.
- Fang X. & Stefan H.G. 1999. Projection of climate change effects on water temperature characteristics of small lakes in the contiguous U.S. *Clim. Change* 42: 377–412.
- Fischlin A., Midgley G.F., Price J.T., Leemans R., Gopal B., Turley C., Rounsevell M.D.A., Dube O.P., Tarazona J. & Velichko A.A. 2007. Ecosystems, their properties, goods, and services. In: Parry M.L., Canziani O.F., Palutikof J.P., van der Linden P.J. & Hanson C.E. (eds.), *Climate change 2007: impacts, adaptation and vulnerability*, Contribution of Working Group II to the Fourth Assessment Report of the Intergovernmental Panel on Climate Change, Cambridge University Press, Cambridge, pp. 211–272.

- Gerdeaux D. 2004. The recent restoration of the whitefish fisheries in Lake Geneva: the roles of stocking, reolimnology, and climate change. *Ann. Zool. Fennici* 41: 181–189.
- Gillet C. & Quetin P. 2006. Effect of temperature changes on the reproductive cycle of roach in Lake Geneva from 1983 to 2001. *J. Fish. Biol.* 69: 518–534.
- Goudsmit G.-H., Burchard H., Peeters F. & Wüest A. 2002. Application of k - ϵ turbulence models to enclosed basins: The role of internal seiches. *J. Geophys. Res.* 107: 3230–3243.
- Goyette S., McFarlane N.A. & Flato G. 2000. Application of the Canadian Regional Climate Model to the Laurentian Great Lakes Regions. Implementation of a Lake Model. *Atmos. Ocean.* 38: 481–503.
- Hambricht K.D., Gophen M. & Serruya S. 1994. Influence of long term climatic changes on the stratification of a tropical, warm monomictic lake. *Limnol. Oceanogr.* 39: 1233–1242.
- Henderson-Sellers B.M., McCormick J. & Scavia D. 1983. A comparison of the formulation for eddy diffusion in two one-dimensional stratification models. *Appl. Math. Model.* 7: 212–215.
- Hodges B., Imberger J., Saggio A. & Winters K.B. 2000. Modeling basin-scale internal waves in a stratified lake. *Limnol. Oceanogr.* 45: 1603–1620.
- Hondzo M. & Stefan H.G. 1991. Three case studies of lake temperature and stratification response to warmer climate. *Water Resour. Res.* 27: 1837–1846.
- Hondzo M. & Stefan H.G. 1993. Regional water temperature characteristics of lakes subjected to climate change. *Clim. Change* 24: 187–211.
- Hostetler S.W. & Bartlein P.J. 1990. Simulation of lake evaporation with application to modelling lake-level variations at Harney-Malheur Lake, Oregon. *Water Resour. Res.* 26: 2603–2612.
- Imberger J., Patterson J.C., Hebbert B. & Loh I. 1978. Dynamics of reservoir of medium size. *J. Fluid Mech.* 78: 489–512.
- IPCC 2001. *Climate change 2001: The scientific basis, vol. 1. The third assessment report of the Intergovernmental Panel on Climate Change (IPCC)*. University Press, Cambridge.
- IPCC 2007. *Climate change 2007: the physical science basis*. Contribution of Working Group I to the Fourth Assessment Report of the Intergovernmental Panel on Climate Change, Cambridge University Press, Cambridge.
- Jacquet S., Briand J.F., Leboulanger C., Oberhaus L., Paolini G., Druart J.C., Anneville O. & Humbert J.F. 2005. The proliferation of the toxic cyanobacterium *Planktothrix rubescens* following restoration of the largest natural French lake (Lake Bourget). *Harmful Algae* 4: 651–672.
- Jöhnk K.D., Huisman J., Sharples J., Sommeijer B., Visser P.M. & Stroom J.M. 2008. Summer heatwaves promote blooms of harmful cyanobacteria. *Glob. Change Biol.* 14: 495–512.
- Jungo P. & Beniston M. 2001. Change in the anomalies of extreme temperature anomalies in the 20th century at Swiss climatological stations located at different latitudes and altitudes. *Theor. Appl. Climatol.* 69: 1–12.
- Kanoshina I., Lips U. & Leppänen J.-M. 2003. The influence of weather conditions (temperature and wind) on cyanobacterial bloom development in the Gulf of Finland (Baltic Sea). *Harmful Algae* 2: 29–41.
- Kelley J.G.W., Hobgood J.S., Bedford K.W. & Schwab D.J. 1998. Generation of Three-dimensional lake model forecasts for Lake Erie. *Weather Forecast.* 13: 659–687.
- King J.R., Shuter B.J. & Zimmerman A.P. 1997. The response of the thermal stratification of South Bay (Lake Huron) to climatic variability. *Can. J. Fish. Aquat. Sci.* 54: 1873–1882.
- King J.R., Shuter B.J. & Zimmerman A.P. 1999. Empirical links between thermal habitat, fish growth and climate change. *Trans. Am. Fish. Soc.* 128: 656–665.
- Kraus E.B. & Turner J.S. 1967. A one dimensional model of the seasonal thermocline: II. The general theory of its consequences. *Tellus* 19: 98–106.
- Lazzarotto J. & Rapin F. 2007. Evolution physico-chimique des eaux du Léman. In: *Rapp. Comm. int. prot. Eaux Léman contre pollut., Campagne 2006*, Commission for the Protection of Lake Geneva, pp. 33–57.
- Lazzarotto J., Rapin F. & Corvi C. 2004. Physical-chemical changes and tests for metals and various micropollutants in the waters of Lake Geneva. In: *Rapp. Comm. Int. prot. Eaux Léman contre pollut., Campagne 2003*, pp. 31–58.
- Lazzarotto J., Nirel P. & Rapin F. 2006. Evolution physico-chimique des eaux du Léman. In: *Rapp. Comm. int. Prot. eaux Léman contre pollut., Campagne 2005*, pp. 31–63.
- Livingstone D.M. 2003. Impact of secular climate change on the thermal structure of a large temperate central European lake. *Clim. Change* 57: 205–225.
- Massey F.J. 1956. The Kolmogorov-Smirnov test for goodness of fit. *J. Am. Stat. Ass.* 46: 68–78.
- McCormick M.J. & Fahnenstiel G.L. 1999. Recent climatic trends in nearshore water temperatures in the St. Lawrence Great Lakes. *Limnol. Oceanogr.* 44: 530–540.
- Mironov D.V. 2008. *Parameterization of lakes in numerical weather prediction. Description of a lake model*. COSMO Technical Report No. 11, Deutscher Wetterdienst, Offenbach am Main, Germany.
- Mironov D., Heise E., Kourzeneva E., Ritter B., Schneider N. & Terzhevik A. 2010. Implementation of the lake parameterisation scheme FLake into the numerical weather prediction model COSMO. *Boreal Env. Res.* 15: 218–230.
- Mortsh L. & Quinn F. 1996. Climate change scenarios for Great Lakes Basin ecosystems studies. *Limnol. Oceanogr.* 41: 903–911.
- Nakicenovic N., Alcamo J., Davis G., de Vries B., Fenhann J., Gaffin S., Gregory K., Grübler A., Jung T.Y., Kram T., La Rovere E.L., Michaelis L., Mori S., Morita T., Pepper W., Pitcher H., Price L., Riahi K., Roehrl A., Rogner H.-H., Sankovski A., Schlesinger M., Shukla P., Smith S., Swart R., van Rooijen S., Victor N. & Dadi Z. 2000. *Special report on emissions scenarios*. Working Group III, Intergovernmental Panel on Climate Change (IPCC), Cambridge University Press, Cambridge.
- Orlob G.T. & Selna L.G. 1970. Temperature variations in deep reservoirs. *J. Hydraul. Div. Proc.* 96: 393–410.
- Peeters F., Straile D., Lorke A. & Livingstone D.M. 2007.

- Earlier onset of the spring phytoplankton bloom in lakes of the temperate zone in a warmer climate. *Glob. Change Biol.* 13: 1898–1909.
- Peeters F., Livingstone D.M., Goudsmit G.-H., Kipfer R. & Forster R. 2002. Modeling 50 years of historical temperature profiles in a large central European lake. *Limnol. Oceanogr.* 47: 186–197.
- Perroud M., Goyette S., Martynov A., Beniston M. & Anneville O. 2009. Simulation of multiannual thermal profiles in deep Lake Geneva: a comparison of one-dimensional lake models. *Limnol. Oceanogr.* 54: 1574–1594.
- Robertson D.M. & Ragotzkie R.A. 1990. Changes in the thermal structure of moderate to large sized lakes in response to changes in air temperature. *Aquat. Sci.* 52: 360–380.
- Roelke D. & Buyukates Y. 2002. The diversity of harmful algal bloom-triggering mechanisms and the complexity of bloom initiation. *Hum. Ecol. Risk Assess.* 7: 1347–1362.
- Schindler D.W., Bayley S.E. & Parker B.R. 1996. The effect of climatic warming on the properties of boreal lakes and streams at the experimental lakes area, northwestern Ontario. *Limnol. Oceanogr.* 41: 1004–1017.
- Shatwell T., Köhler J. & Nicklisch A. 2008. Warming promotes cold-adapted phytoplankton in temperate lakes and opens a loophole for Oscillatoriales in spring. *Glob. Change Biol.* 14: 2194–2200.
- Stefan H.G. & Fang X. 1994. Dissolved oxygen model for regional lake analysis. *Ecol. Model.* 71: 37–68.
- Stefan H.G., Hondzo M. & Fang X. 1993. Lake water quality modeling for projected future climate scenarios. *J. Environ. Qual.* 22: 417–431.
- Stefan H.G., Hondzo M. & Fang X. 1996. Simulated long-term temperature and dissolved oxygen characteristics of lakes in the north-central United States and associated fish habitat limits. *Limnol. Oceanogr.* 41: 1124–1135.
- Stefan, H.G., Fang X. & Hondzo M. 1998. Simulated climate changes effects on year-round water temperatures in temperate zone lakes. *Clim. Change* 40: 547–576.
- Stepanenko V.M. & Lykosov V.N. 2005. Numerical simulation of heat and moisture transport in the “lake-soil” system. *Russian Journal of Meteorology and Hydrology* 3: 95–104.
- Uhlmann B., Goyette S. & Beniston M. 2009. Sensitivity analysis of snow patterns in Swiss ski resorts to shifts in temperature, precipitation and humidity under condition of climate change. *Int. J. Climatol.* 29: 1048–1055.
- Winder M. & Hunter D.A. 2008. Temporal organization of phytoplankton communities linked to physical forcing. *Oecologia* 156: 179–192.
- Yao A.Y.M. 1974. A statistical model for the surface relative humidity. *J. Appl. Meteor.* 13: 17–21.

Appendix

Steps in the development of pseudo-random meteorological data generation extending the series from 10 years to 130 years

Step 1: All values taken by a variable from 1981 to 1990 at 00:00 UTC, x_{i0} ($i = [T, v, RH, dir]$ and $0 = 00:00$ UTC), for each day in a particular month are selected and sorted to determine the shape of the distribution (Fig. A1).

Step 2: A value of m_i is then randomly selected according to the distribution curve defined in step 1 and is given the value m_{i0} (Fig. A2). For instance, a normal distribution would increase the probability to have a m_{i0} close to the mean μ .

Step 3: Values at 01:00 UTC are strongly dependent on the data at 00:00 UTC, those at 02:00 UTC on the data at 01:00 UTC and so on. Unfortunately, the recurrence of this approach (steps 1 and 2) from one hour to the next is not adequate

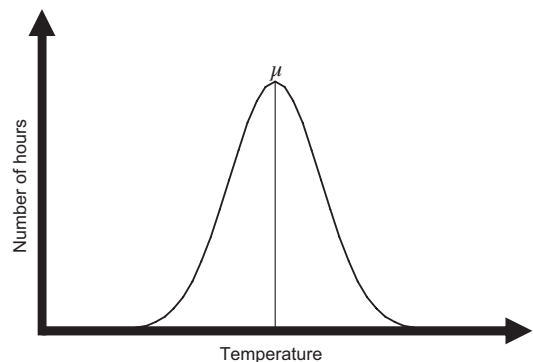


Fig. A1. Temperature normal distribution function over the period 1981–1990 at 00:00 UTC for a particular month. Distributions: T : normal; v : lognormal; dir : multimodal; H : Pearson type 1 (beta) (Yao 1974).

as it would artificially increase intra-day variability. Therefore, the classification method suitable for the distribution at 00:00 UTC partitions the values in different classes. All the data at 00:00 UTC that are in the same class as m_{i0} (Fig. A3) are found and are used to select their

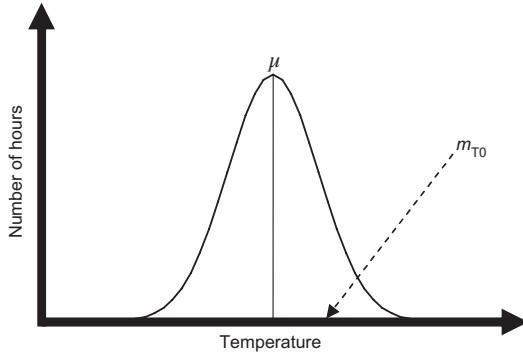


Fig. A2. Choice of a temperature value for m_{T0} according to the distribution function defined in **Fig. 1**.

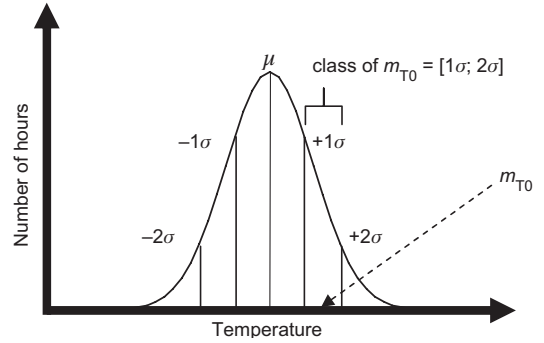


Fig. A3. Selection of values that stand in the same class as m_{T0} . Classification methods: T : classification by mean and standard deviation; v : classification by geometric progressions; dir : Classification by equal amplitudes; H : classification by mean and standard deviation.

respective values at 01:00 UTC.

Step 4: The selected values at 01:00 UTC compose a new dataset, DS_1 (1 for 01:00 UTC) (Fig. A4). The random selection of a value for 01:00 UTC, m_{T1} , must consider the new distribution curve of DS_1 . In DS_1 , T still follows a normal distribution [(a normality test of Kolmogorov-Smirnov (Massey 1956))] but distributions for v , dir and RH are more chaotic and are not related to the original distribution. While a pseudo-random value drawn from the normal distribution in DS_1 is given to m_{T1} , statistical properties of the other variables are used to border the range of possible random values. The procedure for T (steps 3 and 4) is repeated for the following hours, which means that each m_i is evaluated according to the condition that precedes it.

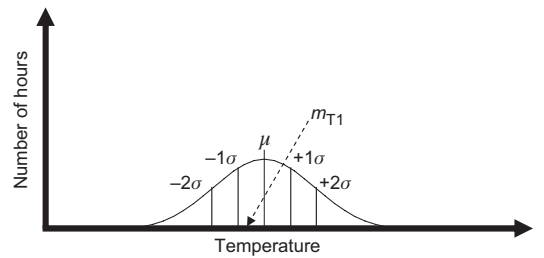


Fig. A4. Choice of a temperature value for m_{T1} according to the temperature distribution curve of DS_1 .

A set of techniques is tested in order to find values for m_{v1-23} and m_{RH1-23} that reasonably reproduce the μ_D , the σ_{IAD} and the σ_{IED} . These include the random selection of a number over a uniform distribution limited by the minimum and maximum or by the $\mu \pm 1, 1.1, \dots, 2\sigma$ of DS_1 , or over a normal distribution defined by parameters of DS_1 . The same procedure is applied to the following hours on the basis of the value selected at the preceding hour. The best results are obtained when m_{v1-23} is drawn randomly from a uniform

distribution in the range $\mu \pm 1.6\sigma$ (Fig. 4) and m_{RH1-23} from a normal distribution (Fig. 4). The selection method for RH has been adopted since more than 90% of the DS_{1-23} follow a normal distribution.

The approach is different for $m_{dir1-23}$ as wind direction does not follow any regular daily pattern. m_{dir0} is randomly chosen between 0° and 360° and m_{dir1} is selected according to the probability of occurrence after a given m_{dir0} . Directions are then partitioned into 16 classes and those to whom m_{dir0} and m_{dir1} belong are defined. Then, the succession of these two classes of directions is searched during the month and m_{dir2} is pseudo-randomly selected based on the occurrence probabilities of each class after such a configuration. The same pattern is then extended to $m_{dir3-23}$.